




# Photometric Analysis of Three Potential Red Nova Progenitors

Surjit S. Wadhwa<sup>1</sup> , Ain De Horta<sup>1</sup>, Miroslav D. Filipović<sup>1</sup>, N. F. H. Tohill<sup>1</sup>, Bojan Arbutina<sup>2</sup>, Jelena Petrović<sup>3</sup>, and Gojko Djurašević<sup>3</sup>

<sup>1</sup> School of Science, Western Sydney University, Locked Bag 1797, Penrith, NSW 2751, Australia; [19899347@student.westernsydney.edu.au](mailto:19899347@student.westernsydney.edu.au)

<sup>2</sup> Department of Astronomy, Faculty of Mathematics, University of Belgrade, Studentski trg 16, 11000 Belgrade, Serbia

<sup>3</sup> Astronomical Observatory, Volgina 7, 11060 Belgrade, Serbia

Received 2022 June 15; revised 2022 July 10; accepted 2022 July 26; published 2022 September 28

## Abstract

We present photometric analysis of three bright red nova progenitor contact binary systems: ASAS J082151-0612.6, TYC 7281-269-1 and TYC 7275-1968-1. The primary components in all three systems are solar-type low mass stars with radii somewhat larger than their zero age main sequence counterparts. The secondaries, as in most contact binary systems, have radii and luminosities well above their main sequence counterparts. All three have extremely low mass ratios ranging from 0.075 to 0.097 and two have high degrees of contact, in excess of 75%. All three have mass ratios and separations below the theoretical values for orbital stability. Chromospheric activity, a hallmark of magnetic activity and magnetic braking, considered important in mediating angular momentum loss, is also explored. All three systems demonstrate the O'Connell effect, and all systems require the introduction of star spots for a better light curve solution. In addition, we show that ASAS J082151-0612.6 and TYC 7281-269-1 have a UV color excess in the range indicating high chromospheric activity. Another measure of potential significant magnetic activity is X-ray luminosity; TYC 7275-1968-1 and probably also TYC 7281-269-1 have X-ray luminosity well above other contact binary systems. We conclude that it is likely that all three are unstable and hence are potential merger candidates.

*Key words:* (stars:) binaries: eclipsing – techniques: photometric – stars: low-mass

## 1. Introduction

Red novae and luminous red novae are likely caused by mergers of components of low-mass contact binary systems. Stellar mergers are likely to be quite common with estimates by Kochanek et al. (2014) suggesting a Galactic rate of about once every decade. V1309 Sco remains the only confirmed merger event although only in retrospect (Tylenda et al. 2011). Pre-merger study of potentially unstable systems is critical to our understanding of the orbital dynamics and internal stellar structure of such systems. Several factors, such as total spin and orbital angular momentum (Rasio 1995), angular momentum loss (Stepień & Gazeas 2012a) and the extent of contact between the components (Rasio & Shapiro 1995), appear to be among the most critical in influencing orbital stability and potential merger. Recently, interest in identification of contact binary star merger candidates has seen renewed activity with new projects exploring observational (Gazeas et al. 2021) and theoretical (Wadhwa et al. 2021) aspects. Among the most studied instability parameters are the link between the mass ratio of the components and orbital stability (Rasio 1995; Arbutina 2007, 2009). Van Noord et al. (2016) pointed out that detecting merger candidates using traditional period analysis would be rather impractical, requiring vast amounts of data acquired over decades. In addition they noted that most sky survey data are unlikely to be useful given

the spread of the observations. The detection of potential red novae candidates thus depends first on the identification of probable candidates utilizing the link between mass ratio and orbital stability and subsequent focused follow up (potentially over many years) observations.

As part of an ongoing project aimed at identifying potential low mass contact binaries with signs of orbital instability, we are in the process of systematically reviewing photometric data from various sky surveys to select potential candidates. As part of our initial review of our algorithm we have identified three potential candidates from the All Sky Automated Survey (ASAS) (Pojmanski 2002). We perform detailed photometric analysis of these and confirm that all three systems exhibit features of orbital instability. Magnetic and chromospheric activity indicators reveal that all three systems are active and likely undergoing angular momentum loss from magnetic braking.

## 2. Observations

Photometric observations of three recently identified contact binary systems were performed: ASAS J082151-0612.6 (A0821), TYC 7281-269-1 (T7281) and TYC 7275-1968-1 (T7275). A0821 ( $\alpha_{2000.0} = 082150.91$ ,  $\delta_{2000.0} = -061238.5$ ) is an ASAS discovery with a period of 0.309334 day and V band amplitude of 0.35 mag. The system was observed over

**Table 1**  
Basic Catalog and Light Curve Parameters for the Three Systems

Name	Mag Range	Obs Num	Exp Time (s)	Distance (pc)	$E(B-V)$	$m_{V1}$	$M_{V1}$
A0821	11.85–12.15 ( <i>V</i> )	257	30	$342.9 \pm 12.1$	0.063	12.12	$4.64 \pm 0.08$
	11.56–11.85 ( <i>R</i> )	250	25				
	12.26–12.58 ( <i>B</i> )	255	50				
T7281	12.08–12.40 ( <i>V</i> )	160	20	$426.4 \pm 11.0$	0.059	12.37	$4.40 \pm 0.06$
	11.78–12.08 ( <i>R</i> )	239	20				
T7275	11.47–11.71 ( <i>V</i> )	154	25	$326.7 \pm 60$	0.059	11.67	$4.28 \pm 0.44$

**Note.**  $m_{V1}$  is the apparent magnitude of the primary at mid-secondary eclipse and  $M_{V1}$  is the calculated absolute magnitude of the primary.

two nights in March 2020. T7281 ( $\alpha_{2000.0} = 140712.98$ ,  $\delta_{2000.0} = -302443.7$ ) is another ASAS discovery with a period of 0.363583 day and *V* band amplitude of 0.23 mag. The system was observed over six nights in June 2020.

T7275 ( $\alpha_{2000.0} = 131559.56$ ,  $\delta_{2000.0} = -370017.7$ ) is a Catalina Sky Survey discovery (Drake et al. 2017) with a period of 0.382807 day and *V* band amplitude of 0.25 mag. The system was recorded by ASAS but not formally recognized as a contact binary. The system was observed over three nights in May and June 2020.

All systems were observed using the 0.6 m telescope at the Western Sydney University Penrith Observatory utilizing an SBIG 8300T CCD camera and Johnson *B*, *V* and *R* filters. The total number of observations for each filter along with exposure times are summarized in Table 1. The American Association of Variable Star Observers (AAVSO) VPHOT engine was employed for plate solving and differential photometry. The VPHOT engine adjusts the aperture radius to 1.5 times the point spread function (PSF) for each image. TYC 4860-905-1 was used as the comparison star and USNO-B1 0838-0176857 as the check star for A0821, 2MASS 14064960-3023173 was used as the comparison star and 2MASS 14073366-3026255 as the check star for T7281 and TYC 7275-1145-1 was used as the comparison and TYC 7275-1587-1 as the check star for T7275. Given the relative brightness of the contact binary systems, we chose comparison stars with similar brightness and color within the available field. We referenced the AAVSO Photometric All Sky Survey (Henden et al. 2018) for the magnitudes of the comparison stars. All observations with estimated error (as provided by VPHOT) exceeding 0.01 mag were excluded. As only a single time of minima of the primary eclipse for each system was acquired, refinement of the ephemeris was not undertaken and data were folded using the ASAS derived periods. We adopted the deeper eclipse as the primary at phase zero and brightest magnitude determined by means of a parabolic fit of the data around phase 0.25 and phase 0.75.

Photometry was acquired in *B*, *V* and *R* bands for A0821, *V* and *R* bands for T7281, and *V* band for T7275. All three systems displayed moderate O’Connell effect with the secondary maxima fainter by 0.03 mag (*V*) for A0821 and 0.02 mag

(*V*) for T7275, while the primary maxima were fainter by 0.03 mag (*V*) for T7281. The basic catalog and our light curve findings for the three systems are summarized in Table 1.

### 3. Light Curve Analysis and Determination of Absolute Parameters

#### 3.1. Light Curve Analysis

We relied on the 2009 version of the Wilson–Devinney (WD) light curve code with Kurucz atmospheres (Wilson & Devinney 1971; Wilson 1990; Kallrath et al. 1998; Nelson 2021) to analyze the photometric data. Complete eclipses are seen in all systems, making them suitable for light curve analysis and determination of the photometric mass ratio (Terrell & Wilson 2005). Given the presence of the O’Connell effect in all three systems, both unspotted and spotted solutions were modeled. The absolute magnitude of the primary was determined using the mid-secondary eclipse apparent visual magnitude along with the distance and reddening as described in Wadhwa et al. (2021). The error in the absolute magnitude was estimated from the reported error in the distance. The effective temperature of the primary was fixed, based on absolute magnitude calibrations from Pecaut & Mamajek (2013). The common envelope suggests that the components should have similar temperatures, so gravity darkening coefficients were fixed,  $g_1 = g_2 = 0.32$  (Lucy 1967), as were bolometric albedos,  $A_1 = A_2 = 0.5$ , and simple reflection treatment was applied (Rucinski 1969). Logarithmic law (Nelson & Robb 2015) limb darkening coefficients for each wavelength were interpolated from van Hamme (1993).

Due to significant correlation between the geometric elements, it is only possible to estimate the mass ratio of a contact binary system (photometrically) in systems with total eclipses (Rucinski 1993; Terrell & Wilson 2005). More recently Liu (2021) has shown the photometric mass ratio error to be in the vicinity of 1% in the presence of total eclipses. The eclipse amplitude and duration constrain the mass ratio and inclination respectively, overcoming these correlations to some extent, and allowing the mass ratio grid search method (or “*q*-search”, Russo & Sollazzo 1982) to be applied to obtain the

mass ratio. The method involves obtaining solutions for various fixed values of  $q$ , with the inclination and potential (fill-out) acting as free parameters. Each solution is then compared to the observed light curve to find the best solution. Light curve solutions of the three systems (simultaneously where multiple bands were acquired) were modeled at mass ratio intervals of 0.01 over the range 0.05 to 0.9. When a preliminary solution was obtained the search was further refined with analysis at mass ratio intervals of 0.001 on either side of the preliminary solution. The best solution was regarded as the likely mass ratio (without a spot). A single spot was introduced by way of trial and error based on the preliminary mass ratio solution and the process repeated again with spot parameters (size, temperature factor and location) also acting as free parameters. The best solution from this set represented the mass ratio with spots. In all cases the spotted solution provided a better fit over the unspotted solution. For the final iteration of the WD code, the mass ratio was also allowed to be a free parameter and the reported standard deviation for each of the variable parameters was adopted as the error for each parameter.

The presence of spots may pose a problem with simultaneous multi-band light curve solutions with inconsistencies between the fitted and observed values. The phenomenon is well recognized, and historical examples include AG Vir (Bell et al. 1990), EH Hya (Samec et al. 1991) and CQ Cep (Demircan et al. 1997) while more recent examples include V781 Tau (Kallrath et al. 2006), MW Pav (Alvarez et al. 2015) and H I Pup (Ulaş & Ulusoy 2014). In the case of H I Pup the authors were unable to find a simultaneous spotted solution and could only solve the blue band with the introduction of a spot. The WD code assigns the same spot parameter values for all pass-bands, but this may not be correct for active stars, where there is evidence of significant flux variation at different wavelengths with respect to stellar magnetic activity (Ballerini et al. 2012). Such variations are likely to introduce fitting errors which cannot be corrected for when attempting to solve multiple pass-bands simultaneously. Solving each band separately may potentially lead to different values for parameters such as the mass ratio, thus introducing potential uncertainty. Simultaneous solutions, when possible, probably lead to the correct mass ratio at the expense of robust fitting between the observed and modeled light curves. Such fitting errors are evident in two of our systems where multiple bands were solved simultaneously. Introduction of additional spots or third light did not improve the overall fit.

Both T7281 and T7275 were found to be extreme low mass ratio systems ( $q = 0.082$  and  $q = 0.075$  respectively) with deep contact (>95% for unspotted solution and >75% for the spotted solutions). There is good thermal contact between the components with only a small difference in component temperatures. A0821 was also found to be an extreme low mass ratio ( $q = 0.097$ ) system in good thermal contact. The degree of contact (38%) is somewhat lower than the other two

systems. The fitted light curves, residuals and mass ratio search grids for the spotted solutions are plotted in Figure 1, with three-dimensional (3D) representations of the systems in Figure 2. The light curve solutions along with absolute and astrophysical parameters (see below) are summarized in Table 2.

In the case of T7281, the secondary is slightly cooler in the unspotted solution, and slightly hotter in the spotted solution. The primary eclipse however does not change, similar to other low mass ratio systems including V1187 Her (Wadhwa 2017), TY Pup (Sarotsakulchai et al. 2018), LO And (Nelson & Robb 2015), V857 Her (Qian & Yang 2005) and ASAS J083241+2332.4 (Sriram et al. 2016). There was no significant change in the mass ratios for T7281 and A0821 with the addition of a spot; however, the best solution for T7275 resulted in an increase in the mass ratio  $q = 0.07$  to  $q = 0.075$  with the addition of the spot. Other variations such as change in inclination, temperature of the secondary and degree of contact between the spotted and unspotted solutions are summarized in Table 2.

### 3.2. Absolute Parameters

Reliable estimates of the absolute parameters can be made if the mass ratio and the absolute magnitude of the primary are known. The absolute magnitude  $M_{V1}$  gives the luminosity of the primary. From the maximum brightness we estimate the luminosity of the system, and hence the luminosity of the secondary can be estimated. It is reasonably well established that the primary components of contact binary systems can be regarded as zero age main sequence (ZAMS) stars (Yildiz & Doğan 2013). The mass of the primary was derived from the ZAMS mass–luminosity relation for stars  $>0.7 M_{\odot}$  (Demircan & Kahraman 1991); the mass ratio then yields the mass of the secondary. Errors for the mass of the primary were estimated from the error in the absolute magnitude (see above). The separation of the component A is derived from Kepler’s third law, expressed as  $(A/R_{\odot})^3 = 74.5(P/\text{days})^2((M_1 + M_2)/M_{\odot})$  with error propagated from the errors in the mass of the components.

The relative radii of the components are not independent as they are enclosed in a common envelope, but are dictated by the mass ratio and Roche geometry. Using the geometric mean of the fractional radii (from three orientations) provided by the light curve solution we estimate the mean volume fractional radius of the primary and secondary ( $r_{1,2}$ ). From  $R_1 = r_1 A$  and  $R_2 = r_2 A$  (Awadalla & Hanna 2005), we derive the mean radii of the components for all three systems. As has been reported previously (Stępień & Gazeas 2012b) the relative luminosity and radii of the secondary were considerably higher than those modeled for main sequence counterparts. The absolute parameters based on the best (spotted) light curve solutions are summarized in Table 2.

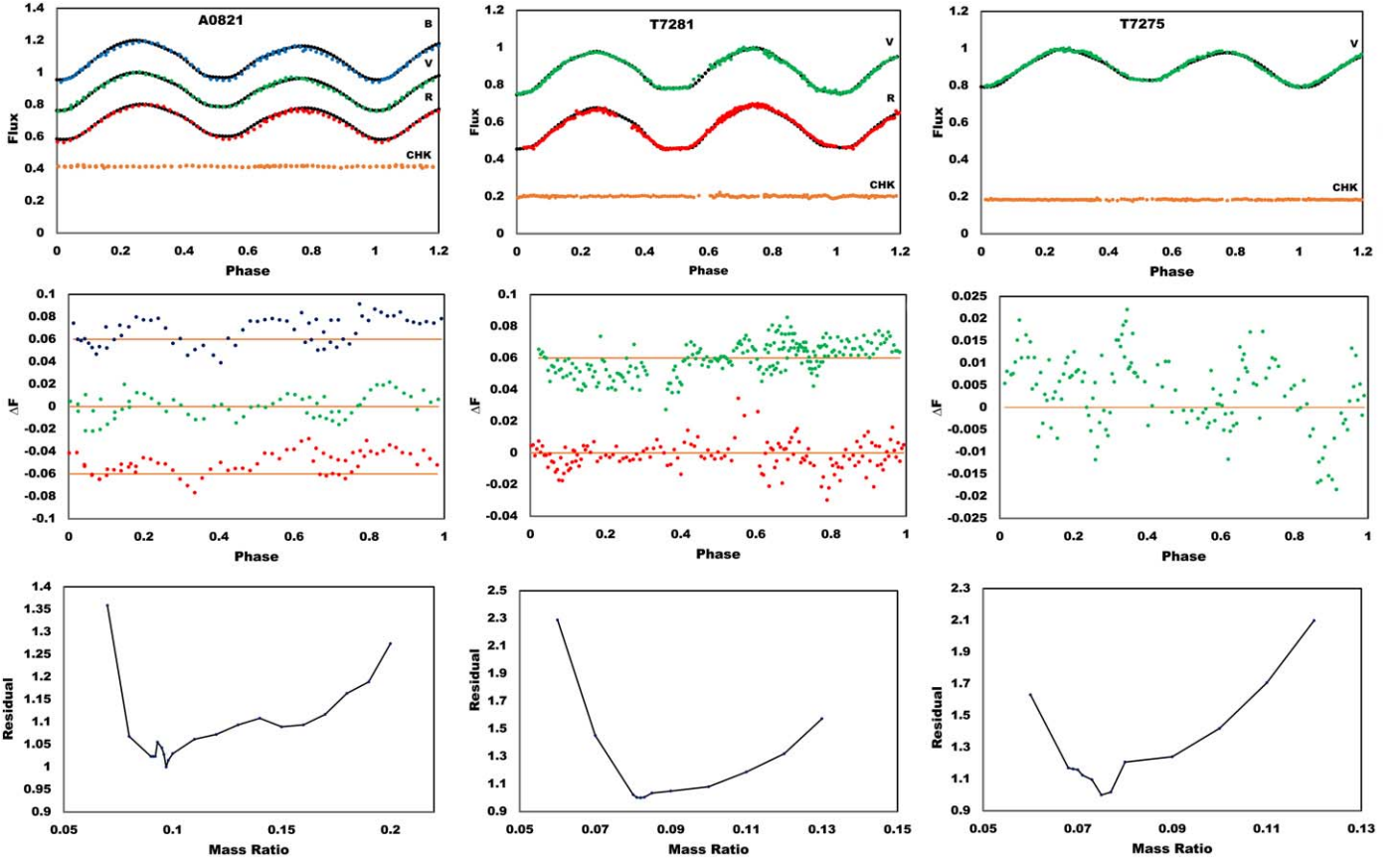


**Figure 1.** Fitted light curves, residuals and mass ratio search grids for A0821 (left), T7281 (center) and T7275 (right). The upper panels display the fitted (black) and observed (colored) light curves of the various bands as labeled. The curves have been normalized to the maximum brightness. In the cases of A0821 and T7281 the non V band curves have been shifted vertically for ease of display. Due to the large number of data points the curves for A0821 have been binned 2:1 for illustration. The middle panels display the residuals for each band as a difference in the normalized flux. Again where there are multiple bands the curves have been shifted vertically for clarity. The bottom panels illustrate the mass ratio search grids for the spotted solutions. The residual error has been normalized to the lowest value for clarity. Similarly for clarity the region near the minimum mass ratio is illustrated.

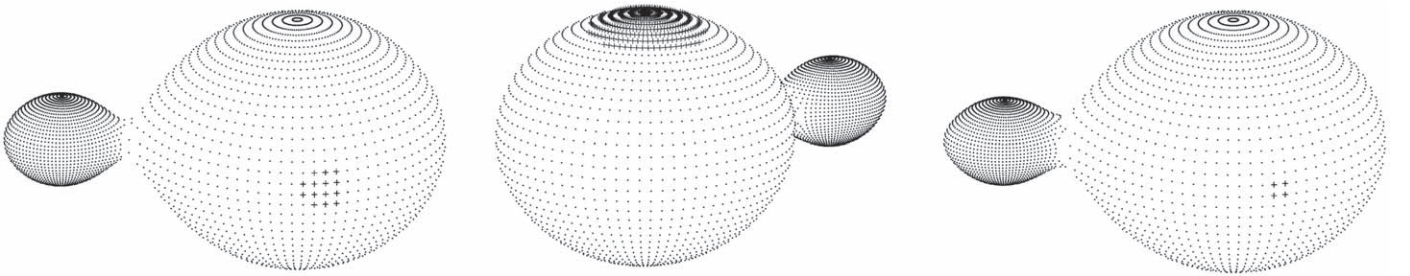


**Figure 2.** 3D representations for ASAS J082151-0612.6 (left), TYC 7281-269-1 (middle) and TYC 7275-1968-1 (right). The spots are drawn as the darker regions. The orientations of the 3D images are slightly altered relative to the light curve solutions to allow visualization of the spots.

## 4. Orbital Stability

### 4.1. Instability Mass Ratio and Separation

Merger of a contact binary system is likely when the combined orbital and spin angular momentum of the system is

at a critical (minimum) value where tidal instability results as described by Darwin (1879). Recently, Wadhwa et al. (2021) showed that the mass ratio ( $q$ ) at the onset of orbital instability is dependent on the mass of the primary star for low mass ( $0.5 M_{\odot} < M < 1.6 M_{\odot}$ ) stars. There is no single

**Table 2**  
Light Curve Solution, Absolute Parameters and Instability Parameters for ASAS J082151-0612.6, TYC 7281-269-1 and TYC 7275-1968-1

Parameter	A0821		T7281		T7275	
	No Spot	Spot	No Spot	Spot	No Spot	Spot
$T_1$ (K) (Fixed)	5850	5850	5960	5960	6010	6010
$T_2$ (K)	$5710 \pm 40$	$5705 \pm 44$	$5840 \pm 45$	$6240 \pm 38$	$5765 \pm 86$	$5615 \pm 65$
Inclination ( $^\circ$ )	$70.06 \pm 1.50$	$70.1 \pm 1.4$	$74.4 \pm 2.0$	$74.2 \pm 1.0$	$68.8 \pm 1.4$	$69.8 \pm 1.5$
Fill-out (%)	$38 \pm 4$	$35 \pm 4$	$99 \pm 1$	$77 \pm 2$	$99 \pm 1$	$83 \pm 2$
$r_1$ (mean)		0.6288		0.6170		0.5242
$r_2$ (mean)		0.2458		0.2230		0.2195
$q$ ( $M_2/M_1$ )	$0.097 \pm 0.010$	$0.097 \pm 0.010$	$0.082 \pm 0.004$	$0.082 \pm 0.004$	$0.070 \pm 0.002$	$0.075 \pm 0.002$
$q_{\text{inst}}$	0.107	0.107	0.105	0.101	0.099	0.098
$A/R_\odot$	$1.99 \pm 0.01$	$1.99 \pm 0.01$	$2.25 \pm 0.01$	$2.25 \pm 0.01$	$2.35 \pm 0.01$	$2.35 \pm 0.01$
$A_{\text{inst}}/R_\odot$	...	2.00	...	2.29	...	2.41
$M_1/M_\odot$	$1.01 \pm 0.01$	$1.01 \pm 0.01$	$1.08 \pm 0.01$	$1.08 \pm 0.01$	$1.11 \pm 0.02$	$1.11 \pm 0.02$
$M_2/M_\odot$	$0.098 \pm 0.002$	$0.098 \pm 0.002$	$0.088 \pm 0.002$	$0.088 \pm 0.002$	$0.078 \pm 0.002$	$0.084 \pm 0.002$
$R_1/R_\odot$		$1.18 \pm 0.02$		$1.39 \pm 0.02$		$1.47 \pm 0.02$
$R_2/R_\odot$		$0.43 \pm 0.01$		$0.50 \pm 0.02$		$0.52 \pm 0.021$
$M_{V1}$		$4.64 \pm 0.08$		$4.40 \pm 0.06$		$4.28 \pm 0.44$
$M_{\text{FUV}}$		14.66		12.82		
$M_{\text{FMS}}$		16.84		16.01		
UV Color Excess		-1.71		-2.69		
<b>Spot Details</b>						
Latitude		90		120		90
Longitude		260		10		250
Radius ( $^\circ$ )		$10.2 \pm 0.6$		$26.7 \pm 0.77$		$5.01 \pm 0.17$
Temp Factor		$1.2 \pm 0.05$		$1.10 \pm 0.01$		$1.38 \pm 0.03$

**Note.** Radii,  $A_{\text{inst}}$ , absolute magnitudes and color excess are only shown for the best fitting (spotted) solutions.

minimum mass ratio at which instability will occur—the instability mass ratio is dependent on the gyration radii of the primary and secondary components. The gyration radius for tidally distorted and rotating ZAMS stars of  $0.4 M_\odot < M < 1.4 M_\odot$  is variable and dependent on the mass of the star, so the instability mass ratio is variable and dependent on the mass of the primary.

Briefly, Wadhwa et al. (2021) demonstrated that by numerically solving Equation (1) below with appropriate values for the gyration radii, it is possible to determine the mass ratio  $q$  at which instability is likely to occur for any given contact binary system

$$\frac{q \frac{k_2^2}{k_1^2} P Q + \sqrt{\left(q \frac{k_2^2}{k_1^2} P Q\right)^2 + 3\left(1 + q \frac{k_2^2}{k_1^2} Q^2\right)\left(q \frac{k_2^2}{k_1^2} P^2 + \frac{q}{(1+q)k_1^2}\right)}}{q \frac{k_2^2}{k_1^2} P^2 + \frac{q}{(1+q)k_1^2}} - \frac{0.6q^{-2/3} + \ln(1 + q^{-1/3})}{0.49q^{-2/3} + 0.15f} = 0, \quad (1)$$

where  $k_{1,2}$  are the gyration radii of the primary and secondary,  $f$  is the fill-out factor ( $0 < f < 1.0$ ) and  $P$  and  $Q$  are defined

similarly to Arbutina (2007)

$$P = \frac{0.49q^{2/3} - 3.26667q^{-2/3}(0.27q - 0.12q^{4/3})}{0.6q^{2/3} + \ln(1 + q^{1/3})}, \quad (2)$$

and

$$Q = \frac{(0.27q - 0.12q^{4/3})(0.6q^{-2/3} + \ln(1 + q^{-1/3}))}{0.15(0.6q^{2/3} + \ln(1 + q^{1/3}))}. \quad (3)$$

If the Roche distorted radius of the primary is known, it is possible to determine the separation at which instability is likely (Arbutina 2007) by

$$\frac{A_{\text{inst}}}{R_1} = \frac{q \frac{k_2^2}{k_1^2} P Q + \sqrt{\left(q \frac{k_2^2}{k_1^2} P Q\right)^2 + 3\left(1 + q \frac{k_2^2}{k_1^2} Q^2\right)\left(q \frac{k_2^2}{k_1^2} P^2 + \frac{q}{(1+q)k_1^2}\right)}}{q \frac{k_2^2}{k_1^2} P^2 + \frac{q}{(1+q)k_1^2}} \quad (4)$$

Landin et al. (2009) modeled values of the gyration radii  $k$  of low mass ( $0.09 M_\odot < M < 3.8 M_\odot$ ) rotating and tidally distorted ZAMS stars. We utilize the data to derive a linear

fit for  $0.6 M_{\odot} < M < 1.4 M_{\odot}$  as follows

$$k_1 = -0.2392M_1 + 0.527, \quad (5)$$

that we use to calculate gyration radius of the primary.

The mass ratio of contact binaries approaching merger is low and so the mass of the secondary is very small. For very low mass stars the totally convective  $n = 1.5$  polytrope should be appropriate, with  $k^2 \approx 0.205$  (Arbutina 2007). Nevertheless, we use Landin et al. (2009) data for  $0.09 M_{\odot} < M < 0.2 M_{\odot}$  stars and derive a linear fit in this range

$$k_2 = -0.1985M_2 + 0.485, \quad (6)$$

which we apply for the secondary. We combine these gyration radii to solve Equations (1) and (4), yielding the instability mass ratio  $q_{\text{inst}}$  and instability separation  $A_{\text{inst}}$  for each system. We used  $q_{\text{inst}}$  rather than the light curve solution mass ratio to calculate the instability separation. All three systems have mass ratios and separations below the critical values where orbital instability is likely, so they are potential merger candidates. The instability parameters are summarized in Table 2.

#### 4.2. Magnetic Activity

Loss of angular momentum from binary systems causes the separation between the components to decrease (Li et al. 2004), and the most likely mechanism for angular momentum loss in contact binary systems is magnetic braking. There is indirect evidence that angular momentum loss from cool contact binaries occurs by way of magnetic stellar winds. Increased chromospheric activity and/or strong ultraviolet (UV) emissions are a hallmark of increased magnetic activity and thus increased potential for magnetic braking and magnetic stellar winds in contact binary systems (Rucinski & Vilhu 1983; Vilhu 1983; Li et al. 2004). There are many magnetic and chromospheric signals associated with contact binaries. The asymmetry in the maxima (O’Connell effect) is the most easily observed light curve feature. Light curve analysis, apart from incorporating star spots, provides little indication of chromospheric activity. Certain spectral emission lines particularly in the high energy bands provide much clearer indicators of enhanced chromospheric activity. Chromospheric emissions in the visual band are swamped by the light of the photosphere; but this is not the case in the far-ultraviolet (FUV) region, especially in the case of low mass dwarfs common among contact binary systems (Smith & Redenbaugh 2010). The Galaxy Evolution Explorer (GALEX) satellite imaged the sky in both the FUV band centered on 1539 Å and near-ultraviolet band (NUV) centered on 2316 Å. Unfortunately the NUV band may be contaminated by photospheric flux and only the FUV band can be relied upon for the detection of chromospheric activity (Smith & Redenbaugh 2010).

The fraction of a star’s emission in the active H and K lines (Noyes et al. 1984) is an accepted measure of chromospheric emission strength. This fraction is normally expressed as

$\log R'_{\text{HK}}$ , with  $\log R'_{\text{HK}} \geq -4.75$  characteristic of a more active star (Henry et al. 1996). Using the large database of  $\log R'_{\text{HK}}$  values of dwarf stars produced by the Mount Wilson HK project (Vaughan et al. 1978; Duncan et al. 1991), Smith & Redenbaugh (2010) matched GALEX FUV magnitudes ( $m_{\text{FUV}}$ ) to the  $\log R'_{\text{HK}}$  for dwarf stars to derive two key relationships

$$(m_{\text{FUV}} - B)_{\text{base}} = 6.73(B - V) + 7.43, \quad (7)$$

which defines  $m_{\text{FUV}} - B$  for stars with the weakest emissions and low activity; and

$$\Delta(m_{\text{FUV}} - B) = (m_{\text{FUV}} - B) - (m_{\text{FUV}} - B)_{\text{base}} \quad (8)$$

defining a color excess. For active stars, i.e., those with  $\log R'_{\text{HK}} \geq -4.75$ , they deduced that the color excess was essentially always less than  $-0.5$  and often less than  $-1.0$ . The opposite was true for less active stars with color excesses significantly higher than  $-0.5$ . In a somewhat broader study, Findeisen et al. (2011) detected a good correlation between high  $\log R'_{\text{HK}}$  values and higher FUV luminosity, and in an earlier study Findeisen & Hillenbrand (2010) estimate absolute FUV magnitudes ( $M_{\text{FMS}}$ ) for single main sequence stars from B8 to M2 spectral types.

All three systems show the O’Connell effect, suggesting the possibility of star spots and all three have a better light curve fit when at least one spot is introduced. Two of the systems were observed by GALEX, so a more detailed examination of the chromospheric/magnetic activity is possible. Reported apparent FUV magnitudes for each system were converted to absolute magnitudes  $M_{\text{FUV}}$  and compared with the absolute GALEX magnitude for single stars ( $M_{\text{FMS}}$ ) of the same mass.  $M_{\text{FUV}}$  for A0821 was 2.18 magnitudes brighter than the corresponding main sequence star, and for T7281 absolute FUV magnitude was 3.19 magnitudes brighter. The UV excess (using published values for  $B$  magnitude) for A0821 is estimated to be  $-1.71$  and for T7281,  $-2.69$ . Both are significantly less than  $-1.0$ , considered the hallmark for chromospherically active stars. The chromospheric activity parameters are summarized in Table 2.

W UMa stars are known X-ray emitters. The X-ray emission mechanism is not well understood but may relate to the synchronous fast rotation of the components and magnetic activity related to the common convective envelope (Gondoin 2004). Stępień et al. (2001) reported on the X-ray properties of 57 contact binary systems from the ROSAT survey and found a median X-ray luminosity ( $\log L_X$ ) of 30.04, with mean of 30.18. Only one of our systems was detected as a point source by ROSAT. T7275 is less than  $20''$  from a ROSAT faint point source (Voges et al. 2000) with a count rate  $3.18 \times 10^{-2} \text{ s}^{-1}$ , which equates to a flux  $f_X = 3.36 \times 10^{-13} \text{ erg cm}^{-2} \text{ ct}^{-1}$  after applying the energy conversion factor detailed in Stępień et al. (2001). Using

$$L_X = 4\pi d^2 f_X, \quad (9)$$

where  $d$  is the distance, we determined  $\log L_X = 30.63$  for T7275, somewhat higher than the mean reported by Stępień et al. (2001), suggesting a more active system.

Two sources in the Swift-XRT Point Source catalog (Evans et al. 2020) coincide to within  $2''$  to the positions of T7275 and T7281 and are likely associated with the contact binary systems. X-ray luminosities for each system using the mean 0.3–10 keV observed flux (power law spectrum) are 30.23 and 30.52, respectively. Although not directly comparable to the ROSAT flux, the X-ray luminosities appear to be significantly elevated above average, again suggesting both systems to be magnetically active and subject to enhanced magnetic braking and angular momentum loss.

## 5. Summary and Conclusions

We present initial photometric analysis of three recently identified bright contact binary systems. All three have extremely low mass ratios ranging from 0.075 to 0.097 with two having very high degree of contact. Estimates of the absolute parameters of the components were made possible by well-established parallax distances. The primary in all cases exhibits properties similar to other ZAMS stars of similar mass, while the secondaries, as is typical in contact binary systems, have larger radius and luminosity than their main sequence counterparts.

Dynamic stability of contact binaries is dependent upon the interplay between spin angular momentum and orbital angular momentum. Stability is only possible if the orbital angular momentum is roughly more than three times the total spin angular momentum (Hut 1980). As was reported (Rasio 1995; Li & Zhang 2006; Arbutina 2007, 2009; Wadhwa et al. 2021), there is a direct link between the mass ratio of a contact binary system and the spin and orbital angular momentum. Orbital instability cannot occur if the mass ratio is above a critical value. The critical mass ratio is dependent on the mass of the primary and unique for each system (Wadhwa et al. 2021). In order to determine if any of the systems is a potential merger (red nova) candidate, we derive the theoretical instability mass ratio and separation for each system, compare them with current mass ratios and separations derived from the light curve analysis, and show that all three exhibit criteria suggestive of orbital instability.

As noted by Li et al. (2004), the most likely mechanism of angular momentum loss (and hence potential orbital instability) in contact binary systems is magnetic braking. UV and X-ray observations of contact binary systems (Rucinski & Vilhu 1983; Vilhu 1983) have demonstrated that contact binary systems are strong UV and X-ray sources indicating the presence of a magnetic field and probable active magnetic braking. We look at the chromospheric and magnetic activity as a de facto marker for potential angular momentum loss and find that all three systems have at least some features of enhanced chromospheric

activity. Two systems observed by GALEX show signs of significant chromospheric activity with absolute FUV magnitudes significantly brighter than comparable main sequence single stars and UV color excess well into the range considered to represent increased activity. Two systems also display evidence for significant X-ray emission, also a marker of significant chromospheric and magnetic activity.

Variation in period has been suggested as a marker of orbital instability, however, variation is commonly observed, and as pointed out by Liu et al. (2018), both increasing and decreasing variations in contact binary periods are observed equally. The variations may be due to apsidal motion, light travel time effects, magnetic activity cycles or mass transfer/loss, while the long term period decrease is usually due to angular momentum loss (Liu et al. 2018). None of the systems reported in this study have historical high cadence observations to mount a meaningful short term period study analysis as a marker for orbital instability. In addition, due to the competing mechanisms just mentioned, using period study as an identifier of potential orbital instability is quite impractical.

Given these findings, we believe that all three systems are likely to be unstable and are potential red nova progenitors. The time frame from the onset of instability to eventual merger is unknown. Photometric data for V1309 Sco were available for approximately 6 yr prior to the merger event, and among the most critical changes determined retrospectively were the exponential decline in the period of the V1309 Sco progenitor particularly in the three years prior to merger and the shape of the light curve, especially with respect to the secondary maxima in the six years prior to the merger event (Tylenda et al. 2011). Identification of potential merger candidates and their study prior to the merger event is critical to our understanding of contact binary evolution. Given the relative brightness of these three potential red nova progenitors, long term follow-up monitoring of period and light curve changes can be made with modest equipment and could potentially be performed by advanced amateurs through organizations such as the AAVSO.

## Acknowledgments

This study was based on data acquired on the Western Sydney University Penrith Observatory telescope. We acknowledge the traditional custodians of the land on which the Observatory stands, the Dharug people, and pay our respects to elders past and present.

B.A. acknowledges the financial support of the Ministry of Education, Science and Technological Development of the Republic of Serbia through contract No. 451-03-68/2022-14/200104.

J.P. and G.D. gratefully acknowledge financial support of the Ministry of Education, Science and Technological

Development of the Republic of Serbia through contract No. 451-03-9/2021-14/200002.

This research has made use of the SIMBAD database, operated at CDS, Strasbourg, France.

### ORCID iDs

Surjit S. Wadhwa  <https://orcid.org/0000-0002-7011-7541>

### References

- Alvarez, G. E., Sowell, J. R., Williamon, R. M., & Lapasset, E. 2015, *PASP*, **127**, 742
- Arbutina, B. 2007, *MNRAS*, **377**, 1635
- Arbutina, B. 2009, *MNRAS*, **394**, 501
- Awadalla, N. S., & Hanna, M. A. 2005, *JKAS*, **38**, 43
- Ballerini, P., Micela, G., Lanza, A. F., & Pagano, I. 2012, *A&A*, **539**, A140
- Bell, S. A., Rainger, P. P., & Hilditch, R. W. 1990, *MNRAS*, **247**, 632
- Darwin, G. H. 1879, *Obs*, **3**, 79
- Demircan, O., Ak, H., Ozdemir, S., Tanriver, M., & Albayrak, B. 1997, *AN*, **318**, 267
- Demircan, O., & Kahraman, G. 1991, *Ap&SS*, **181**, 313
- Drake, A. J., Djorgovski, S. G., Catelan, M., et al. 2017, *MNRAS*, **469**, 3688
- Duncan, D. K., Vaughan, A. H., Wilson, O. C., et al. 1991, *ApJS*, **76**, 383
- Evans, P. A., Page, K. L., Osborne, J. P., et al. 2020, *ApJS*, **247**, 54
- Findeisen, K., & Hillenbrand, L. 2010, *AJ*, **139**, 1338
- Findeisen, K., Hillenbrand, L., & Soderblom, D. 2011, *AJ*, **142**, 23
- Gazetas, K. D., Loukaidou, G. A., Niarchos, P. G., et al. 2021, *MNRAS*, **502**, 2879
- Gondoin, P. 2004, *A&A*, **426**, 1035
- Henden, A. A., Levine, S., Terrell, D., et al. 2018, AAS Meeting, 232, 223.06
- Henry, T. J., Soderblom, D. R., Donahue, R. A., & Baliunas, S. L. 1996, *AJ*, **111**, 439
- Hut, P. 1980, *A&A*, **92**, 167
- Kallrath, J., Milone, E. F., Breinhorst, R. A., et al. 2006, *A&A*, **452**, 959
- Kallrath, J., Milone, E. F., Terrell, D., & Young, A. T. 1998, *ApJ*, **508**, 308
- Kochanek, C. S., Adams, S. M., & Belczynski, K. 2014, *MNRAS*, **443**, 1319
- Landin, N. R., Mendes, L. T. S., & Vaz, L. P. R. 2009, *A&A*, **494**, 209
- Li, L., Han, Z., & Zhang, F. 2004, *MNRAS*, **355**, 1383
- Li, L., & Zhang, F. 2006, *MNRAS*, **369**, 2001
- Liu, L. 2021, *PASP*, **133**, 084202
- Liu, L., Qian, S. B., & Xiong, X. 2018, *MNRAS*, **474**, 5199
- Lucy, L. B. 1967, *ZAp*, **65**, 89
- Nelson, R. H. 2021, *NewA*, **86**, 101565
- Nelson, R. H., & Robb, R. M. 2015, *IBVS*, **6134**, 1
- Noyes, R. W., Hartmann, L. W., Baliunas, S. L., Duncan, D. K., & Vaughan, A. H. 1984, *ApJ*, **279**, 763
- Pecaut, M. J., & Mamajek, E. E. 2013, *ApJS*, **208**, 9
- Pojmanski, G. 2002, *AcA*, **52**, 397
- Qian, S., & Yang, Y. 2005, *MNRAS*, **356**, 765
- Rasio, F. A. 1995, *ApJL*, **444**, L41
- Rasio, F. A., & Shapiro, S. L. 1995, *ApJ*, **438**, 887
- Rucinski, S. 1969, *PoAst*, **17**, 163
- Rucinski, S. M. 1993, *PASP*, **105**, 1433
- Rucinski, S. M., & Vilhu, O. 1983, *MNRAS*, **202**, 1221
- Russo, G., & Sollazzo, C. 1982, *A&A*, **107**, 197
- Samec, R. G., Charlesworth, S. D., & Dewitt, J. R. 1991, *AJ*, **102**, 688
- Sarotsakulchai, T., Qian, S. B., Soonthornthum, B., et al. 2018, *AJ*, **156**, 199
- Smith, G. H., & Redenbaugh, A. K. 2010, *PASP*, **122**, 1303
- Sriram, K., Malu, S., Choi, C. S., & Vivekananda Rao, P. 2016, *AJ*, **151**, 69
- Stepień, K., Schmitt, J. H. M. M., & Voges, W. 2001, *A&A*, **370**, 157
- Stepień, K., & Gazetas, K. 2012a, *AcA*, **62**, 153
- Stepień, K., & Gazetas, K. 2012b, in IAU Symposium, Vol. 282, From Interacting Binaries to Exoplanets: Essential Modeling Tools, ed. M. T. Richards & I. Hubeny, **456**
- Terrell, D., & Wilson, R. E. 2005, *Ap&SS*, **296**, 221
- Tylenda, R., Hajduk, M., Kamiński, T., et al. 2011, *A&A*, **528**, A114
- Ulaş, B., & Ulusoy, C. 2014, *NewA*, **31**, 56
- van Hamme, W. 1993, *AJ*, **106**, 2096
- Van Noord, D., Molnar, L., Kinemuchi, K., et al. 2016, *SASS*, **35**, 121
- Vaughan, A. H., Preston, G. W., & Wilson, O. C. 1978, *PASP*, **90**, 267
- Vilhu, O. 1983, *HiA*, **6**, 643
- Voges, W., Aschenbach, B., Boller, T., et al. 2000, *IAU Circ.*, **7432**, 3
- Wadhwa, S. S. 2017, *JAVSO*, **45**, 11
- Wadhwa, S. S., De Horta, A., Filipović, M. D., et al. 2021, *MNRAS*, **501**, 229
- Wilson, R. E. 1990, *ApJ*, **356**, 613
- Wilson, R. E., & Devinney, E. J. 1971, *ApJ*, **166**, 605
- Yildiz, M., & Doğan, T. 2013, *MNRAS*, **430**, 2029